Molecular Microbiology (2015) 95(5), 875–884 ■
doi:10.1111/mmi.12908
First published online 30 January 2015

# *Yersinia enterocolitica* type III secretion injectisomes form regularly spaced clusters, which incorporate new machines upon activation

**Mikhail Kudryashev,[1,2*†] Andreas Diepold,[3**†] Marlise Amstutz,[2] Judith P. Armitage,[3] Henning Stahlberg[1‡] and Guy R. Cornelis[2,4§]**
[1]*Center for Cellular Imaging and NanoAnalytics (C-CINA), Biozentrum, University Basel, WRO-1058, Mattenstrasse 26, Basel 4058, Switzerland.*
[2]*Focal Area Infection Biology, Biozentrum, University of Basel, Klingelbergstrasse 50/70, Basel 4056, Switzerland.*
[3]*Department of Biochemistry, University of Oxford, South Parks Road, Oxford OX1 3QU, UK.*
[4]*Research Unit in Microorganism Biology, University of Namur, 61 rue de Bruxelles, 5000, Namur, Belgium.*

## Summary

**Bacterial type III secretion systems or injectisomes are multiprotein complexes directly transporting bacterial effector proteins into eukaryotic host cells. To investigate the distribution of injectisomes in the bacterium and the influence of activation of the system on that distribution, we combined *in vivo* fluorescent imaging and high-resolution *in situ* visualization of *Yersinia enterocolitica* injectisomes by cryo-electron tomography. Fluorescence microscopy showed the injectisomes as regularly distributed spots around the bacterial cell. Under secreting conditions (absence of $Ca^{2+}$), the intensity of single spots significantly increased compared with non-secreting conditions (presence of $Ca^{2+}$), in line with an overall up-regulation of expression levels of all components. Single injectisomes observed by cryo-electron tomography tended to cluster at distances less than 100 nm, suggesting that the observed fluorescent spots correspond to evenly distributed clusters of injectisomes, rather than single injectisomes. The up-regulation of injectisome components led to an increase in the number of injectisomes per cluster rather than the formation of new clusters. We suggest that injectisome clustering may allow more effective secretion into the host cells.**

Accepted 12 December, 2014. For correspondence. *E-mail mikhail.kudryashev@unibas.ch; Tel. +41-61-387 32 32; Fax +41-61-387 39 86. **E-mail andreas.diepold@bioch.ox.ac.uk; Tel. +44-1865-611315; Fax +44-1865-613201. ‡E-mail henning.stahlberg@unibas.ch; Tel. +41-61-387 32 62; Fax. +41-61-387 39 86. §E-mail guy.cornelis@unamur.be; Tel. +32-81-724401; Fax +32-81-724297. †Indicates equal contribution.

## Introduction

The bacterial type III secretion apparatus, also called injectisome, allows Gram-negative bacteria to export effector proteins directly from the bacterial cytosol to a eukaryotic host cell (Cornelis and Wolf-Watz, 1997; Hueck, 1998; Galan and Collmer, 1999; Cornelis and Van Gijsegem, 2000; Hayes *et al.*, 2010; Buttner, 2012). The effectors modulate the function of regulatory molecules in the eukaryotic cell to the benefit of the bacterium and are often essential for pathogenesis or symbiosis (Viprey *et al.*, 1998; Alfano and Collmer, 2004; Mota and Cornelis, 2005; Grant *et al.*, 2006; Coburn *et al.*, 2007; Dean, 2011).

The injectisome is a complex nanomachine spanning both bacterial membranes and extending from the cytosol to the extracellular space. Its assembly involves some 25 different proteins (Cornelis, 2006; Galan and Wolf-Watz, 2006), most of them forming the structure and the others acting as ancillary components driving the assembly (Diepold and Wagner, 2014). The injectisome is evolutionary related to the bacterial flagellum, with which it shares about 10 conserved proteins forming the basic type III secretion export apparatus (Blocker *et al.*, 2003; Macnab, 2004; Cornelis, 2006; Minamino and Namba, 2008; Erhardt *et al.*, 2010). In the bacterial membranes, the injectisome resembles a barrel created by three multimeric protein rings (YscCDJ in *Yersinia*). Five inner membrane proteins (YscRSTUV) form an export apparatus, which is located at the cytoplasmic face of the inner membrane ring formed by YscDJ. The export apparatus is implicated in substrate recognition and has been proposed to form the actual gate for export across the bacterial membranes. On the cytosolic side, five proteins are conserved and essential for type III secretion: an ATPase, YscN, and its negative regulator, YscL, a homolog of the flagellar C ring, YscQ, which interacts with a less-studied component, YscK, and YscO, which structurally resembles the FoF1 stalk (Pallen *et al.*, 2006). The injectisome extends to the extracellular space with a hollow needle assembled through helical

polymerization of a small protein (YscF) (Cordes *et al*., 2003; Deane *et al*., 2006). The function of the needle is to bridge the space between the bacterial outer membrane and the host cell plasma membrane (Mota *et al*., 2005). This space is determined by the extracellular domains of membrane-anchored proteins such as the adhesin YadA that forms a ~ 30 nm thick coat around *Yersinia enterocolitica* (Hoiczyk *et al*., 2000) and the respective binding partners on the host cell (Mota *et al*., 2005; Mikula *et al*., 2012). The needle terminates with a pentameric tip structure (formed by LcrV in *Yersinia*) serving as a scaffold for the formation of a pore in the host cell membrane (Mueller *et al*., 2005; Veenendaal *et al*., 2007; Montagner *et al*., 2011). Isolated subcomplexes of the injectisome, so-called 'needle complexes' containing the needle and the membrane rings, were analyzed to almost molecular detail by a combination of high-resolution methods (Schraidt and Marlovits, 2011; Bergeron *et al*., 2013). Recently, cryo-electron tomography (cryo-ET) revealed an intermediate resolution structure of the injectisomes *in situ* (Kawamoto *et al*., 2013; Kudryashev *et al*., 2013), which showed remarkable structural variation between single machines (Kudryashev *et al*., 2013).

Upon contact to a host cell, a cytosolic mechanism, which prevents the premature export of effector proteins, is released (Yother and Goguen, 1985; Forsberg and Wolf-Watz, 1988; Ferracci *et al*., 2005) and the effectors are translocated into the host cell (Rosqvist *et al*., 1994; Sory and Cornelis, 1994). In *Yersinia*, this can be mimicked by incubation of bacteria in calcium-depleted medium, where the effectors are then secreted into the supernatant (Michiels *et al*., 1990). Under these 'secreting' conditions, the expression of injectisome subunits and the formation of needles are increased (Allaoui *et al*., 1995; Stainier *et al*., 1997; Mueller *et al*., 2005), most likely because of the export of two negative regulators, YscM1 and YscM2 (Stainier *et al*., 1997). However, the effect of this up-regulation on the formation of injectisomes has not as yet been analyzed.

To address this question and to determine the distribution of injectisomes, their integration into the membrane and the influence of external conditions, we combined fluorescence microscopy, capable of detecting the overall distribution of injectisomes *in vivo* in various functional states, with cryo-ET, which allows direct visualization of single injectisomes at nanometer scale in 3D. In this study, we show that the distribution of injectisomes on the surface of *Y. enterocolitica* is not random but that single injectisomes cluster within distances of 100 nm. These clusters are evenly distributed around the bacterial surface. While the number of clusters only slightly increases upon induction of secretion, the number of injectisomes per cluster is increased under secreting conditions by 73–79%.

## Results

### *Expression of injectisome components and formation of needles increase upon activation of the system*

In order to quantify the up-regulation of synthesis of type III secretion system (T3SS) components upon induction of secretion by chelation of $Ca^{2+}$ (Allaoui *et al*., 1995; Stainier *et al*., 1997) and to analyze its impact on the localization of injectisomes, we analyzed both the expression levels and the distribution and intensity of fluorescent injectisome foci under secreting and non-secreting conditions (presence of 5 mM Ethylenediaminetetraacetic acid (EDTA) or 5 mM $Ca^{2+}$ respectively). We quantified the expression of various components covering different structural (Fig. 1A) and functional parts of the injectisome by immunoblots of total cellular protein (Fig. 1B): the needle subunit YscF and tip LcrV, the ruler protein YscP, the inner membrane ring components YscD and YscJ, and the cytosolic C-ring component YscQ. In addition, we quantified the needles formed by assaying YscF and LcrV from purified needles (Mueller *et al*., 2005). All expression levels as well as the amount of purified needle protein were up-regulated about twofold (up-regulation range: 56–145%, Fig. 1B and C) 3 h after induction of the T3SS under secreting vs. non-secreting conditions (Fig. 1B and C). This ratio stayed relatively constant over time (Fig. 1B and C).

### *Activation of the T3SS increases the intensity rather than the number of injectisome foci*

To test the effect on injectisome distribution in live bacteria, we identified and analyzed the foci formed by EGFP-YscD, YscV-mCherry and EGFP-YscQ. The fusion proteins expressed from the native genetic background are stable and functional (Diepold *et al*., 2010; Diepold *et al*., 2015) and cover three different functional parts of the injectisome: the rings, the export apparatus and the cytosolic components respectively. The number and intensities of fluorescent foci in fluorescent Z-stacks were automatically estimated using a simple routine based on geometry and image statistics (Fig. 2A and *Experimental Procedures*). We analyzed the functional labeled components under secreting and non-secreting conditions (Fig. 2B). For all tested components, the spots were 73 to 79% more intense under secreting conditions, indicating a higher number of subunits per spot (Fig. 2C). As previously suggested for EGFP-YscQ (Diepold *et al*., 2010), the number of spots changed less. The average number of detected fluorescent spots per 1 μm of bacterial length was 3.8 under non-secreting and 4.9 under secreting conditions (a statistically significant increase of 29%, $P = 6e{-}5$).

### *Cryo-ET of* Y. enterocolitica *injectisomes*

Because the overall stoichiometry of each injectisome is unlikely to change between non-secreting and secreting

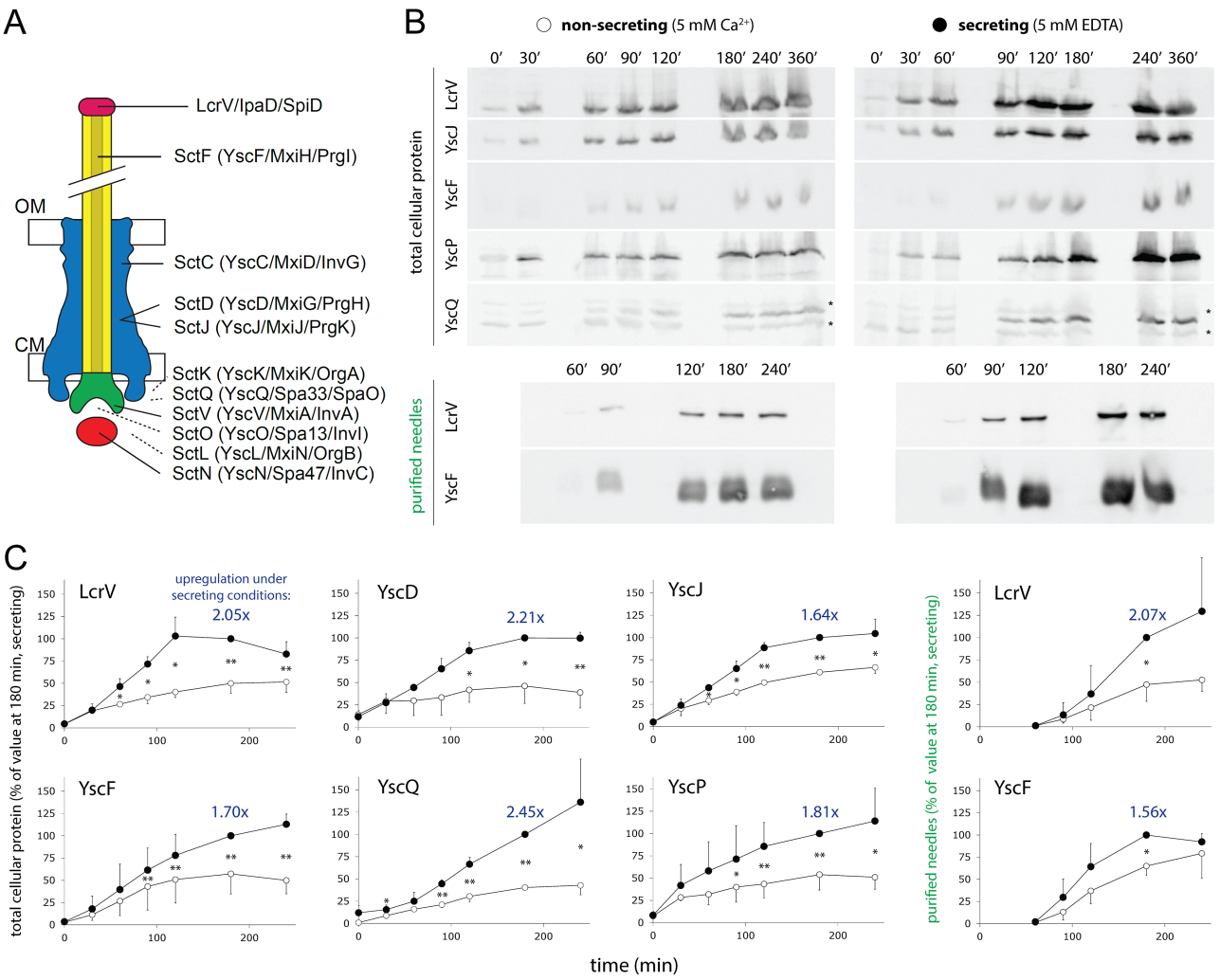


**Fig. 1.** Cellular protein levels of various injectisome components and the amount of needles are similarly influenced by extracellular calcium levels and develop likewise over time.
A. Scheme of the injectisome structural components with the proteins marked according to the general Sct nomenclature (Hueck, 1998) as well as the specific protein names in *Yersinia*, *Shigella* and *Salmonella* SPI-1.
B. Immunoblot time course analysis of protein amounts in the total cell fraction and in purified needles, under non-secreting conditions (BHI + 5 mM of $Ca^{2+}$, left side) and secreting conditions (BHI + 5 mM of EDTA, right side) at the indicated time after induction of the T3SS by temperature shift to 37°. Asterisks denote unspecific bands in the immunoblot.
C. Quantitative analysis of expression levels based on immunoblot intensities. The 180 min value in secreting conditions has been set as 100%. Numbers indicate the increase in protein levels under secreting conditions vs. non-secreting conditions 180 min after induction of the T3SS. Asterisks denote the statistical significance of the protein levels under both conditions for each given time point (*$P < 0.05$; **$P < 0.01$ in a one-tailed, paired sample Student's *t*-test). Open circles, non-secreting conditions; filled circles, secreting conditions. Measurements from three to five independent experiments.

conditions, the results presented above suggest that fluorescent foci can correspond to more than one injectisome. Fluorescent foci that are located within ~ 300 nm away from each other cannot be spatially resolved because of the diffraction limit (Heilemann, 2010). Localization of single injectisomes is only made possible by imaging at the nanometer scale resolution. Therefore, we analyzed the distribution of *Y. enterocolitica* injectisomes and their integration within the bacterial cell envelope in detail by cryo-ET. We imaged secreting and non-secreting regularly sized *Y. enterocolitica* cells and previously described secreting minicells (Kudryashev *et al.*, 2013), where the injectisomes are more readily visualized. Injectisomes of similarly prepared minicells of *Salmonella typhimurium* were shown to be functional (Carleton *et al.*, 2013). Minicells studied by cryo-ET exhibited mostly spherical shapes of ~ 250–350 nm radius in the imaging plane, while the wild-type (*wt*) *Yersinia* bacteria showed elongated shapes of a few micrometers in length and 600–800 nm in width. The vertical dimensions of these cells on vitrified cryo electron

 

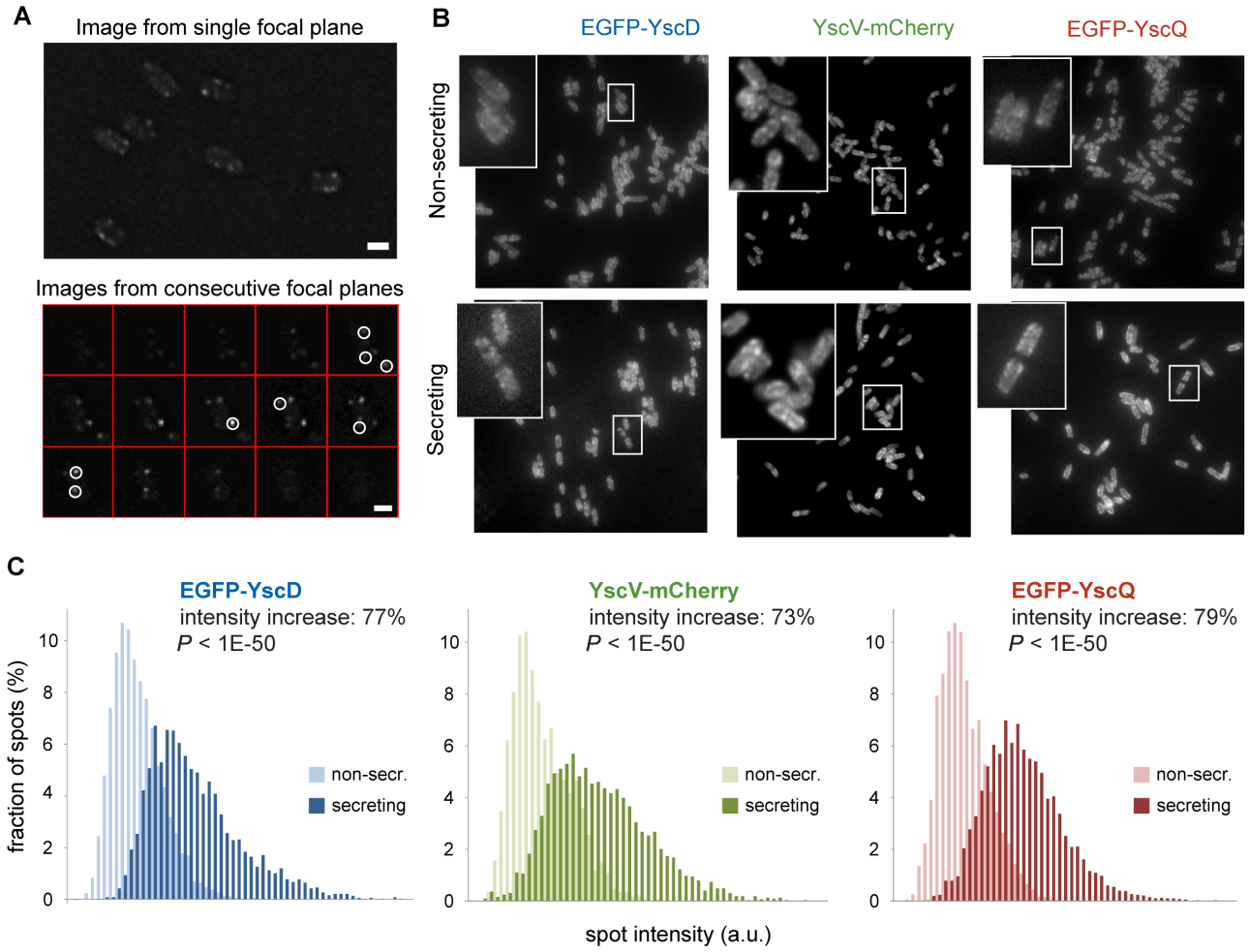


**Fig. 2.** The intensity of injectisome foci is increased upon activation of the type III secretion system.
A. Image from single focal plane within a microscopy 3D stack with *Yersinia enterocolitica* expressing EGFP-YscQ from the native genetic environment (top). Images from consecutive focal planes (top to bottom, d = 150 nm) with automatically detected foci marked with circles in the slices corresponding to the middle of the fluorescent intensity (bottom). All the foci are detected in 3D. Scale bars: 1 μm.
B. Representative fluorescence microscopy images of strains expressing EGFP-YscD, YscV-mCherry and EGFP-YscQ from their native genetic environment, under non-secreting conditions (top) and secreting conditions (bottom). Image width: 50 μm. Insets are three times magnified.
C. Histograms representing the distribution of spot intensities of the bacterial constructs analyzed above. Per strain and condition, more than 2300 individual foci from more than 350 individual cells were analyzed. The *Y* axis represents the fraction of foci in an intensity bin (bin size: 8.3% of average intensity of spots under non-secreting conditions).

microscopic grids are slightly thinner, because of the cell flattening from the layer of vitreous ice, resulting in vertical diameters of ~ 200–300 nm for some minicells and 500–700 nm for *wt* bacteria (Fig. 3). Injectisomes could be clearly localized to the lateral edges of the bacteria in tomographic 3D reconstructions (Fig. 3A and B). In contrast to conventional EM preparations (Kubori *et al.*, 1998; 2000), the outer membranes were smooth and continuous around the injectisome basal bodies (Fig. 3A and B) and did not invaginate, similar to the recent cryo-visualizations of the injectisomes of other bacteria (Kawamoto *et al.*, 2013; Nans *et al.*, 2014; Pilhofer *et al.*, 2014). The inner membrane of the bacteria in the vicinity of injectisomes looks smooth in the examined *Yersinia* cells as well as in *Salmonella* (Kawamoto *et al.*, 2013), while some of the inner membranes around cryo-preserved *Chlamydia*, *Simkania* and *Parachlamydia* injectisomes were invaginating (Nans *et al.*, 2014; Pilhofer *et al.*, 2014). The basal bodies of most of the injectisomes were traversing the bacterial peptidoglycan layer ~ 5 nm below the outer membrane (Fig. 3B). Some bacteria showed two periplasmic layers instead of one. These two layers were equally spaced between the cytoplasmic and outer membranes (Fig. 3C), and evoked previous observations for other Gram-negative bacterial species (Hoffmann *et al.*, 2008; Murphy *et al.*, 2008). In these cases, the top periplasmic layer was

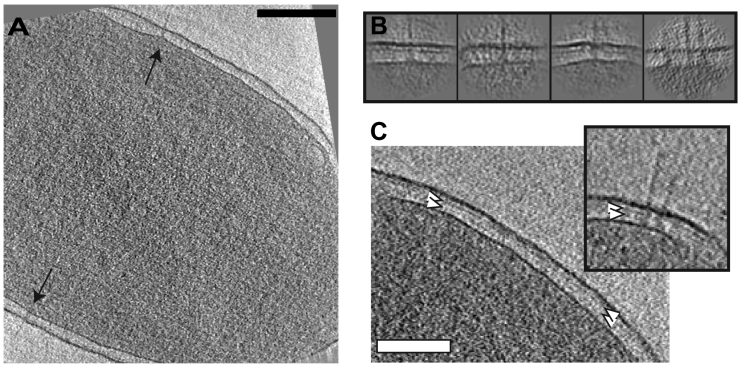


**Fig. 3.** *In situ* visualization of the *Yersinia enterocolitica* injectisomes.
A. A 20 nm thick section through a cryo-electron tomogram of a regular-sized *Y. enterocolitica* cell. Black arrows indicate injectisomes. Scale bar: 300 nm.
B. Typical single and paired injectisomes. Box size: 200 nm.
C. A 30 nm thick section through a tomogram of a regular-sized *Y. enterocolitica* cell showing two periplasmic layers (white arrowheads). Scale bar: 100 nm; inset: paired injectisomes traversing two periplasmic layers.

traversed by the injectisome basal body at the level of periplasmic domain of YscC multimer, while the second layer was traversed close to the bacterial inner membrane (Fig. 3C, inset).

### *Injectisome distribution on the surface of bacteria*

By cryo-ET, we observed a tendency of injectisomes to occur in pairs (Fig. 3B and C) and in larger groups (Fig. 4A). Using coordinates of the injectisomes in tomograms, we simulated fluorescent micrographs by reducing the observable resolution to 300 nm. This resulted in merging of the nearby injectisomes into foci that were well distributed around the cell perimeter (Fig. 4B), similar to the actual fluorescent images (Fig. 2A and B). Up to five injectisomes were observed per one simulated focus (i.e. third example from Fig. 4B). While in tomograms of regular-sized bacteria under secreting conditions we observed on average 6.2 injectisomes per tomogram ($n = 249$), non-secreting bacteria had 3.3 injectisomes ($n = 14$). Imaged secreting minicells showed on average 2.9 injectisomes ($n = 141$). The largest number of injectisomes that we observed was 28 per tomogram of one regular-sized secreting cell. Statistical analysis of 1941 injectisome coordinates from 390 tomograms showed that injectisomes had a tendency to cluster within distances shorter than ~100 nm to each other on the surface of the bacteria in regular cells and in minicells (Fig. 4C). To test if such a distribution pattern could arise by chance, we modeled a random distribution of injectisomes on the surface of hypothetical spherical cells, which are good approximations for minicells. During the simulation, we accounted for the imaging geometry of cryo-ET (see *Experimental procedures*). The number of injectisomes per cell was determined by analyzing the cryo-ET volumes (above and Fig. 4). Injectisomes that were randomly distributed over the surface had a most probable value for a distance of ~ 400 nm (Fig. 4C, black), which was significantly different from the situation observed for the data for both WT and minicells of *Yersinia* (Fig. 4C, blue and red) but similar to the values for non-secreting bacteria (Fig. 4C, green graph). In the random distribution simulation, the probability to find injectisomes within 100 nm to each other was under 5%, whereas it was 21% for injectisomes observed in minicells. On the other hand, a large fraction of injectisome-to-injectisome distances tended to locate 'as far as possible' with an apparent secondary peak at ~ 650 nm for minicells, which is similar to the minicell diameter. This peak is missing for the regular-sized cells, which are larger and less regular shaped. The presence of this secondary peak may represent a tendency of injectisome clusters to localize farther away from each other and more evenly spread across the membrane than to be expected by chance.

## Discussion

In this manuscript, we provide evidence that *Y. enterocolitica* injectisomes cluster within the bacterial membrane and that the up-regulation of synthesis of injectisome components upon activation of the system leads to an increase in the number of injectisomes per cluster, rather than in the number of clusters per bacterium.

The number of injectisomes observed by cryo-ET underestimates the real value by a factor of about two, because of the missing wedge problem in electron tomography (Lucic *et al.*, 2005), which renders the injectisomes on the top and bottom membranes of bacteria hard to visualize. Regular-sized bacteria could not be fully imaged with cryo-ET at the desired magnification. The field of view of our tomograms is $\sim 1.5 \times 1.5\ \mu m^2$. Because of shifts between the images during tomographic data collection, some of the volume close to the edges of the tomogram is not usable. Thus, our estimate of the effective length of an imaged bacterium in a tomogram is 1 μm. This suggests the presence of around two and a half injectisomes per fluorescent spot (6.2 injectisomes per tomogram * 2 underestimation factor / 1 μm of bacterial length per tomogram / 4.9 average foci per 1 μm of length = 2.5 injectisomes per spot) on average under secreting conditions,

 

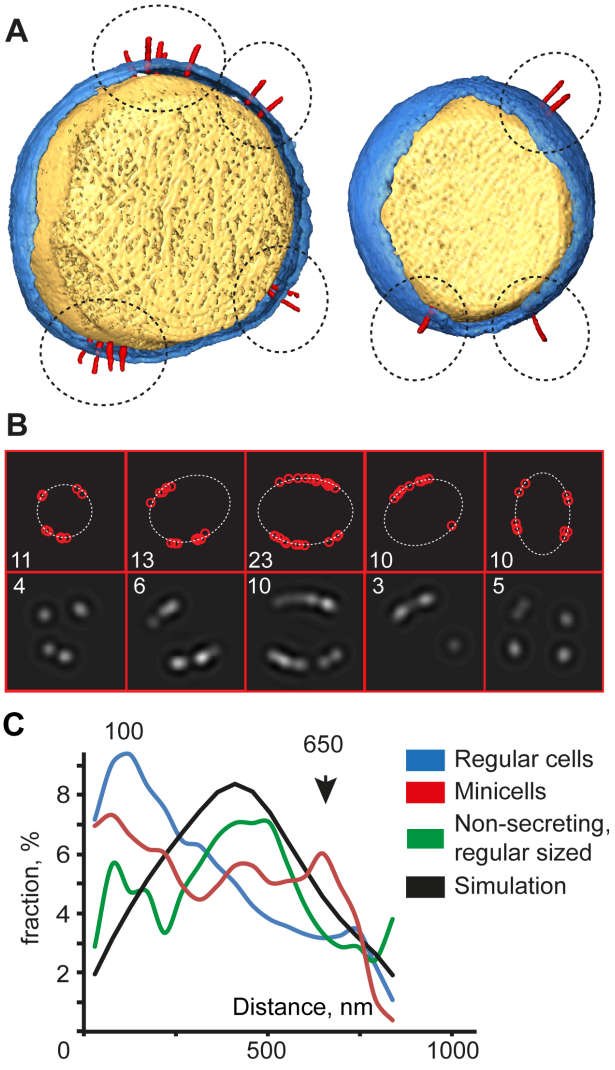


**Fig. 4.** Non-random distribution of injectisomes on the surface of *Yersinia enterocolitica* cells.
A. Volume-rendered representations of two round *Y. enterocolitica* cells (left: incidental small wild-type cell; right: a minicell) with cytoplasm in yellow, bacterial outer membrane in blue and injectisomes in red. Clusters of the injectisomes are marked with dashed black circles. The larger cell was shown previously (Kudryashev *et al.*, 2013).
B. Top: Sketch of injectisome distribution for five bacteria detected from cryo-ET. Cell edge is marked by white ellipses; injectisomes are marked with red circles. Bottom: Light microscopic image simulated from the top panel by limiting the resolution to 300 nm. Numbers represent the number of injectisomes identified by cryo-ET (top) and number of foci in a slice of the simulated light microscopy image (bottom). Box size: 2.5 μm.
C. Frequencies of encounter of the pair distances between the injectisomes as measured from tomograms (green, blue and red lines). Black line: From simulation assuming random distribution of injectisomes with the same number of injectisome per cell.

while the observed maximum is five injectisomes per focus. Because a fraction of needles might have been lost during sample handling for EM preparation, this value represents the lower boundary of our estimation.

There may be several mechanisms of regulation of injectisome clustering. First, the assembly of new injectisomes may be restricted to defined places in the membranes. The secretin YscC is the first protein to assemble within the bacterial membranes (Diepold *et al.*, 2010) and penetrates the peptidoglycan layer. While in other T3SSs, dedicated lytic transglycosylases encoded in the respective pathogenicity islands can locally degrade the peptidoglycan to allow for insertion of the secretin (Koraimann, 2003). *Yersinia* does not have such an enzyme and integration of new injectisomes may therefore be restricted to sites of peptidoglycan remodeling. Another option is that the integration site of the secretin into the peptidoglycan layer is determined by the localization of its pilotin protein (YscW in *Yersinia*), a lipoprotein that is required for the oligomerization and correct localization of YscC (Koster *et al.*, 1997; Burghout *et al.*, 2004a,b). To our knowledge, cellular distribution of YscW has not been investigated. Finally, it is possible that injectisomes exert a physical force onto the membranes that would favor closer localization of the molecular complexes spanning them. We have previously shown that injectisomes *in situ* show a ~ 40% elongation compared with their isolated versions (Kudryashev *et al.*, 2013), indicating that *in situ*, the injectisomes may exert a pulling force on the outer and inner membranes to bring those membranes closer together. Injectisomes in cluster formation would distribute the required force, making the cluster arrangement energetically more favorable. Such energy minimization lends to a simple physical explanation for cluster formation, implying that injectisomes move after synthesis laterally into the vicinity of other injectisomes, thereby forming clusters. Interestingly, injectisomes in *Chlamydia trachomatis* cluster on one pole of the cell, enabling multiple contacts to the host cell (Nans *et al.*, 2014). However, *Y. enterocolitica* has multiple clusters of injectisomes potentially maximizing the chance of injectisome contact to the host cell. The exact mechanism of clustering may be a combination of the mentioned biophysical and cell biological contributions.

Our results suggest that the up-regulation of synthesis of injectisome subunits upon activation of the T3SS occurs rather uniformly for all components. Importantly, they also show that this up-regulation results in a higher number of injectisomes per cluster (which is increased by 73–79%), while the increase in the number of cluster foci is less pronounced (29% on average). This suggests that new injectisomes are preferentially located close to the existing ones. The 75% increase is in qualitative agreement with the 88% increase of the number of injectisomes per cell detected by cryo-ET (6.2 vs. 3.3 injectisomes per cell). Injectisomes translocate effector proteins into host cells. This translocation occurs surprisingly quickly after contact to the host cell is established. In *Salmonella*, it has been shown that effectors are translocated with a rate of

up to a thousand molecules per minute (Schlumberger *et al*., 2005) and that the complete cytosolic pool of an effector was translocated within a few minutes. Presumably, such a fast translocation leads to a strong response, thereby minimizing the risk of the bacteria being detected and attacked by the immune system. The clustering of injectisomes shown in our study provides a possible mechanism to increase translocation rates. All injectisomes within a cluster are probably in contact with the host cell simultaneously, translocating effectors in parallel. On the other hand, the regularly spaced distribution of injectisome foci across the cell maximizes the chance that such a contact with the target cell can be established. If these two factors – increasing the probability of cell contact and translocation vs. increasing the translocation rates – indeed govern injectisome clustering, different bacterial species that employ the T3SS in different ways should display various degrees of clustering, ranging from low clustering in bacteria that do not require high translocation rates to strong clustering in species that rely on fast translocation of effectors. Studying the number and distribution of injectisomes in different species might therefore yield valuable insights into how different bacteria employ the same tool, their type III secretion injectisome.

## Experimental procedures

### *Bacterial strains*

All used bacterial strains are described in Supporting Information Table S1. *Y. enterocolitica* IML421asd (Kudryashev *et al*., 2013) is a multi-effector knockout biosafety level 1 derivative of *Y. enterocolitica* E40 (Sory *et al*., 1995). Bacteria were routinely grown at 25°C in brain heart infusion (BHI) containing nalidixic acid (35 μg $ml^{-1}$). To allow growth of *asd* mutant strains, the medium was supplemented with meso-diaminopimelic acid (mDAP) (50 μg $ml^{-1}$).

### Y. enterocolitica *cultures for type III secretion and microscopy analysis*

Cultures were inoculated at an optical density ($OD_{600}$) of 0.12–0.2 in BHI broth either supplemented with 5 mM of $CaCl_2$ and filtered through a 0.45 μm filter tip (non-secreting conditions) or 5 mM of EDTA (secreting conditions), containing glycerol (4 mg $ml^{-1}$ = 43.5 mM), $MgCl_2$ (20 mM), nalidixic acid (35 μg $ml^{-1}$ = 0.138 mM) and mDAP (50 μg $ml^{-1}$ = 0.263 mM). After 90–120 min of growth at 25°C, induction of the *yop* regulon was performed by shifting the culture to 37° (Cornelis *et al*., 1987). Unless stated otherwise, cells were incubated at 37°C for 2 h (for cryo-ET) or 3 h (for all other analyses).

### *Quantification of protein expression levels*

Immunoblots for the time course analysis were performed as described in Diepold *et al*. (2011) using total cellular protein of 0.3 $ODu_{600nm}$ of bacteria. Immunoblots were imaged digitally on a G:Box XX6 (Syngene, Cambridge, UK) and subsequently quantified using ImageJ (NIH, http://imagej.nih.gov/ij/). The signal intensity of the region around the respective protein size in each lane of the immunoblot was normalized, using the background intensity of the immunoblot and the value 180 min after induction of the T3SS under secreting conditions as lower and upper boundaries. The statistical significance of the differences between proteins levels under secreting and non-secreting conditions was determined using a paired one-tailed *t*-test.

### *Fluorescence microscopy*

For fluorescence imaging, about 2 μl of bacterial culture was placed on a microscope slide layered with a pad of 2% agarose in Phosphate buffered saline (PBS). A Deltavision Spectris optical sectioning microscope (Applied Precision, Issaquah, WA, USA) equipped with a UPlanSApo 100×/1.40 oil objective (Olympus, Tokyo, Japan) and a coolSNAP HQ CCD camera (Photometrics, Tucson, AZ, USA) was used to take differential interference contrast (DIC) and fluorescence photomicrographs.

For fluorophore visualization, either the GFP/hsGFP filter set (Ex 475/28 nm, Em 522/44 nm) or the mCherry/hsCherry filter set (Ex 575/25 nm, Em 634/63 nm) was used. DIC frames were taken with 0.05 s and fluorescence frames with 1.0 s exposure time. Per image, a Z-stack containing 15 frames per wavelength with a spacing of 150 nm was acquired. The stacks were deconvolved using softWoRx 5.5 with standard settings (Applied Precision). A representative DIC frame and the corresponding fluorescence frame were selected and further processed with the ImageJ software. Downstream analysis was performed on the non-deconvolved raw data.

### *Automated fluorescent spots counting*

Spot counting was performed in Matlab, supported by the electron tomography-related Dynamo toolbox (Castano-Diez *et al*., 2012) (http://dynamo-em.org/). The idea behind spot detection is separating the high-intensity spots from the cytosolic background using image statistics. First, for every bacterium in the Z-stacks stacks, two tips of the cell were manually selected (in the fluorescent channel). Fluorescence intensities for single bacteria were extracted from Z-stacks, the voxel values outside of the bacterium were masked out and the brightest voxels were found. The vicinity of the brightest spot was further erased with a Gaussian smoothed blur after which the next brightest voxel was found in the loop. The procedure was stopped when the intensity of the brightest spot was below *average+5*standard_deviation* of the voxels for the entire stack. For each spot, we extracted the average value in the sphere of three-pixel (304 nm) radius around the brightest voxel. A Matlab script can be found in Supporting Information Appendix S1. Per strain and condition, more than 2300 spots from more than 350 individual cells were analyzed. The intensity of each individual spot was corrected for the extracellular background, and intensities under secreting and non-secreting conditions were compared.

### *Sample preparation for cryo-ET*

Bacterial cultures were gently spun at 300 *g* for 5 min and bacteria were washed with PBS to a final volume of 20 μl to which 1 μl of 10 nm beads gold was added as markers for further 3D reconstruction. Three microliters of solution was deposited on Quantifoil grids (Quantifoil Micro Tools GmbH, Jena, Germany) with 3.5 μm holes separated by 1 μm carbon film (3.5/1) and were plunge frozen into liquid ethane cooled down to liquid nitrogen temperature with FEI Vitrobot MK4.

### *Cryo-ET*

For imaging of regular-sized *Y. enterocolitica* cells, we used focal pair tomography (Kudryashev *et al*., 2012): two tomograms were acquired for each imaged bacteria first with underfocus of 2 μm ('low defocus') followed by 15 μm ('high defocus'), using the FEI batch tomography tool on an FEI Titan Krios equipped with a Tridem Gatan Image Filter (GIF) and US1000 post-GIF Charge Coupled Device (CCD). The total dose used for each tomogram was kept below 10 k electrons $nm^{-2}$, aiming at an angular coverage of 120° in 41 steps of 3°. *Yersinia* minicells were imaged with the nominal underfocus of 6 μm with 2-degree angular step and the electron dose kept under 15 k electrons $nm^{-2}$. The pixel size was 0.74 nm. Tilt series were aligned using gold marker fiducials using Etomo (Kremer *et al*., 1996) and reconstructed by weighted back projection using Dynamo scripts (Castano-Diez *et al*., 2012). Tomograms with poor alignment parameters were discarded; a total of 249 tomograms of regular-sized cells and 141 tomograms of minicells in secreting state and 14 tomograms from non-secreting bacteria were used. In the mentioned datasets, we detected 1510, 410 and 46 injectisomes correspondingly. Volume-rendered visualizations were produced semi-automatically with Amira (http://www.amira.com).

### *Distance distribution simulation*

For the graph for Fig. 4C, we simulated distances between randomly distributed injectisomes on the surface of a hypothetical bacteria. The idea is placing injectisomes on a surface of spheres in a random position; the number of placed injectisomes per sphere is taken from the real observed data. The radii of the spheres were 350 nm, resembling the radius at the tip of a bacterium. Simulating two angles with radial angle ranging from 0° to 360°, and azimuthal angles ranging from –60° to 60°. Limiting azimuthal angles was performed to simulate the lower detection probability at the top and bottom of minicells due to the missing wedge problem. Azimuthal angles were limited to the range of –60° to 60° to simulate the lower detection probability at the top and bottom of minicells because of the missing wedge problem. Regular Euclidean distances between the injectisomes were measured from these generated positions. The simulation was performed 1000 times and the average values are presented.

## Acknowledgements

We gratefully acknowledge expert assistance with electron microscopy and valuable discussions from Bill Anderson, Kenneth N. Goldie and Mohamed Chami. AD is the recipient of an EMBO long-term fellowship (ALTF 170-2011). This work was in part supported by the Swiss National Science Foundation (SNF 3100AOB-128659 to GRC, SNF Sinergia CRSII3_125110, NCCRs Struct. Biol., Nano and TransCure), the Swiss Initiative for Systems Biology (SystemsX.ch)

The authors declare to have no conflicting interests.

## References

Alfano, J.R., and Collmer, A. (2004) Type III secretion system effector proteins: double agents in bacterial disease and plant defense. *Annu Rev Phytopathol* **42:** 385–414.

Allaoui, A., Schulte, R., and Cornelis, G.R. (1995) Mutational analysis of the Yersinia enterocolitica virC operon: characterization of yscE, F, G, I, J, K required for Yop secretion and yscH encoding YopR. *Mol Microbiol* **18:** 343–355.

Bergeron, J.R., Worrall, L.J., Sgourakis, N.G., DiMaio, F., Pfuetzner, R.A., Felise, H.B., *et al*. (2013) A refined model of the prototypical Salmonella SPI-1 T3SS basal body reveals the molecular basis for its assembly. *PLoS Pathog* **9:** e1003307.

Blocker, A., Komoriya, K., and Aizawa, S. (2003) Type III secretion systems and bacterial flagella: insights into their function from structural similarities. *Proc Natl Acad Sci USA* **100:** 3027–3030.

Burghout, P., Beckers, F., de Wit, E., van Boxtel, R., Cornelis, G.R., Tommassen, J., and Koster, M. (2004a) Role of the pilot protein YscW in the biogenesis of the YscC secretin in Yersinia enterocolitica. *J Bacteriol* **186:** 5366–5375.

Burghout, P., van Boxtel, R., Van Gelder, P., Ringler, P., Muller, S.A., Tommassen, J., and Koster, M. (2004b) Structure and electrophysiological properties of the YscC secretin from the type III secretion system of Yersinia enterocolitica. *J Bacteriol* **186:** 4645–4654.

Buttner, D. (2012) Protein export according to schedule: architecture, assembly, and regulation of type III secretion systems from plant- and animal-pathogenic bacteria. *Microbiol Mol Biol Rev* **76:** 262–310.

Carleton, H.A., Lara-Tejero, M., Liu, X., and Galan, J.E. (2013) Engineering the type III secretion system in non-replicating bacterial minicells for antigen delivery. *Nat Commun* **4:** 1590.

Castano-Diez, D., Kudryashev, M., Arheit, M., and Stahlberg, H. (2012) Dynamo: a flexible, user-friendly development tool for subtomogram averaging of cryo-EM data in high-performance computing environments. *J Struct Biol* **178:** 139–151.

Coburn, B., Sekirov, I., and Finlay, B.B. (2007) Type III secretion systems and disease. *Clin Microbiol Rev* **20:** 535–549.

Cordes, F.S., Komoriya, K., Larquet, E., Yang, S., Egelman, E.H., Blocker, A., and Lea, S.M. (2003) Helical structure of the needle of the type III secretion system of Shigella flexneri. *J Biol Chem* **278:** 17103–17107.

Cornelis, G., Laroche, Y., Balligand, G., Sory, M.P., and Wauters, G. (1987) Yersinia enterocolitica, a primary model for bacterial invasiveness. *Rev Infect Dis* **9:** 64–87.

Cornelis, G.R. (2006) The type III secretion injectisome. *Nat Rev Microbiol* **4:** 811–825.

Cornelis, G.R., and Van Gijsegem, F. (2000) Assembly and

function of type III secretory systems. *Annu Rev Microbiol* **54:** 735–774.
Cornelis, G.R., and Wolf-Watz, H. (1997) The Yersinia Yop virulon: a bacterial system for subverting eukaryotic cells. *Mol Microbiol* **23:** 861–867.
Dean, P. (2011) Functional domains and motifs of bacterial type III effector proteins and their roles in infection. *FEMS Microbiol Rev* **35:** 1100–1125.
Deane, J.E., Roversi, P., Cordes, F.S., Johnson, S., Kenjale, R., Daniell, S., *et al.* (2006) Molecular model of a type III secretion system needle: implications for host-cell sensing. *Proc Natl Acad Sci USA* **103:** 12529–12533.
Diepold, A., and Wagner, S. (2014) Assembly of the bacterial type III secretion machinery. *FEMS Microbiol Rev* **38:** 802–822.
Diepold, A., Amstutz, M., Abel, S., Sorg, I., Jenal, U., and Cornelis, G.R. (2010) Deciphering the assembly of the Yersinia type III secretion injectisome. *EMBO J* **29:** 1928–1940.
Diepold, A., Wiesand, U., and Cornelis, G.R. (2011) The assembly of the export apparatus (YscR,S,T,U,V) of the Yersinia type III secretion apparatus occurs independently of other structural components and involves the formation of an YscV oligomer. *Mol Microbiol* **82:** 502–514.
Diepold, A., Kudryashev, M., Delalez, N.J., Berry, R.M., and Armitage, J.P. (2015) Composition, Formation, and Regulation of the Cytosolic C-ring, a Dynamic Component of the Type III Secretion Injectisome. *PLoS biology* **13** (1), e1002039-e1002039.
Erhardt, M., Namba, K., and Hughes, K.T. (2010) Bacterial nanomachines: the flagellum and type III injectisome. *Cold Spring Harb Perspect Biol* **2:** a000299.
Ferracci, F., Schubot, F.D., Waugh, D.S., and Plano, G.V. (2005) Selection and characterization of *Yersinia pestis* YopN mutants that constitutively block Yop secretion. *Mol Microbiol* **57:** 970–987.
Forsberg, A., and Wolf-Watz, H. (1988) The virulence protein Yop5 of *Yersinia pseudotuberculosis* is regulated at transcriptional level by plasmid-plB1-encoded trans-acting elements controlled by temperature and calcium. *Mol Microbiol* **2:** 121–133.
Galan, J.E., and Collmer, A. (1999) Type III secretion machines: bacterial devices for protein delivery into host cells. *Science* **284:** 1322–1328.
Galan, J.E., and Wolf-Watz, H. (2006) Protein delivery into eukaryotic cells by type III secretion machines. *Nature* **444:** 567–573.
Grant, S.R., Fisher, E.J., Chang, J.H., Mole, B.M., and Dangl, J.L. (2006) Subterfuge and manipulation: type III effector proteins of phytopathogenic bacteria. *Annu Rev Microbiol* **60:** 425–429.
Hayes, C.S., Aoki, S.K., and Low, D.A. (2010) Bacterial contact-dependent delivery systems. *Annu Rev Genet* **44:** 71–90.
Heilemann, M. (2010) Fluorescence microscopy beyond the diffraction limit. *J Biotechnol* **149:** 243–251.
Hoffmann, C., Leis, A., Niederweis, M., Plitzko, J.M., and Engelhardt, H. (2008) Disclosure of the mycobacterial outer membrane: cryo-electron tomography and vitreous sections reveal the lipid bilayer structure. *Proc Natl Acad Sci USA* **105:** 3963–3967.
Hoiczyk, E., Roggenkamp, A., Reichenbecher, M., Lupas, A., and Heesemann, J. (2000) Structure and sequence analysis of Yersinia YadA and Moraxella UspAs reveal a novel class of adhesins. *EMBO J* **19:** 5989–5999.
Hueck, C.J. (1998) Type III protein secretion systems in bacterial pathogens of animals and plants. *Microbiol Mol Biol Rev* **62:** 379–433.
Kawamoto, A., Morimoto, Y.V., Miyata, T., Minamino, T., Hughes, K.T., Kato, T., and Namba, K. (2013) Common and distinct structural features of *Salmonella* injectisome and flagellar basal body. *Sci Rep* **3:** 3369.
Koraimann, G. (2003) Lytic transglycosylases in macromolecular transport systems of Gram-negative bacteria. *Cell Mol Life Sci* **60:** 2371–2388.
Koster, M., Bitter, W., de Cock, H., Allaoui, A., Cornelis, G.R., and Tommassen, J. (1997) The outer membrane component, YscC, of the Yop secretion machinery of *Yersinia enterocolitica* forms a ring-shaped multimeric complex. *Mol Microbiol* **26:** 789–797.
Kremer, J.R., Mastronarde, D.N., and McIntosh, J.R. (1996) Computer visualization of three-dimensional image data using IMOD. *J Struct Biol* **116:** 71–76.
Kubori, T., Matsushima, Y., Nakamura, D., Uralil, J., Lara-Tejero, M., Sukhan, A., *et al.* (1998) Supramolecular structure of the *Salmonella typhimurium* type III protein secretion system. *Science* **280:** 602–605.
Kubori, T., Sukhan, A., Aizawa, S.I., and Galan, J.E. (2000) Molecular characterization and assembly of the needle complex of the *Salmonella typhimurium* type III protein secretion system. *Proc Natl Acad Sci USA* **97:** 10225–10230.
Kudryashev, M., Stahlberg, H., and Castano-Diez, D. (2012) Assessing the benefits of focal pair cryo-electron tomography. *J Struct Biol* **178:** 88–97.
Kudryashev, M., Stenta, M., Schmelz, S., Amstutz, M., Wiesand, U., Castano-Diez, D., *et al.* (2013) In situ structural analysis of the *Yersinia enterocolitica* injectisome. *Elife* **2:** e00792.
Lucic, V., Forster, F., and Baumeister, W. (2005) Structural studies by electron tomography: from cells to molecules. *Annu Rev Biochem* **74:** 833–865.
Macnab, R.M. (2004) Type III flagellar protein export and flagellar assembly. *Biochim Biophys Acta* **1694:** 207–217.
Michiels, T., Wattiau, P., Brasseur, R., Ruysschaert, J.M., and Cornelis, G. (1990) Secretion of Yop proteins by *Yersiniae*. *Infect Immun* **58:** 2840–2849.
Mikula, K.M., Kolodziejczyk, R., and Goldman, A. (2012) *Yersinia* infection tools – characterization of structure and function of adhesins. *Front Cell Infect Microbiol* **2:** 169.
Minamino, T., and Namba, K. (2008) Distinct roles of the FliI ATPase and proton motive force in bacterial flagellar protein export. *Nature* **451:** 485–488.
Montagner, C., Arquint, C., and Cornelis, G.R. (2011) Translocators YopB and YopD from *Yersinia enterocolitica* form a multimeric integral membrane complex in eukaryotic cell membranes. *J Bacteriol* **193:** 6923–6928.
Mota, L.J., and Cornelis, G.R. (2005) The bacterial injection kit: type III secretion systems. *Ann Med* **37:** 234–249.
Mota, L.J., Journet, L., Sorg, I., Agrain, C., and Cornelis, G.R. (2005) Bacterial injectisomes: needle length does matter. *Science* **307:** 1278.

Mueller, C.A., Broz, P., Muller, S.A., Ringler, P., Erne-Brand, F., Sorg, I., *et al*. (2005) The V-antigen of Yersinia forms a distinct structure at the tip of injectisome needles. *Science* **310:** 674–676.

Murphy, G.E., Matson, E.G., Leadbetter, J.R., Berg, H.C., and Jensen, G.J. (2008) Novel ultrastructures of *Treponema primitia* and their implications for motility. *Mol Microbiol* **67:** 1184–1195.

Nans, A., Saibil, H.R., and Hayward, R.D. (2014) Pathogen-host reorganization during *Chlamydia* invasion revealed by cryo-electron tomography. *Cell Microbiol* **16:** 1457–1472.

Pallen, M.J., Bailey, C.M., and Beatson, S.A. (2006) Evolutionary links between FliH/YscL-like proteins from bacterial type III secretion systems and second-stalk components of the FoF1 and vacuolar ATPases. *Protein Sci* **15:** 935–941.

Pilhofer, M., Aistleitner, K., Ladinsky, M.S., Konig, L., Horn, M., and Jensen, G.J. (2014) Architecture and host interface of environmental chlamydiae revealed by electron cryotomography. *Environ Microbiol* **16:** 417–429.

Rosqvist, R., Magnusson, K.E., and Wolf-Watz, H. (1994) Target cell contact triggers expression and polarized transfer of *Yersinia* YopE cytotoxin into mammalian cells. *EMBO J* **13:** 964–972.

Schlumberger, M.C., Muller, A.J., Ehrbar, K., Winnen, B., Duss, I., Stecher, B., and Hardt, W.D. (2005) Real-time imaging of type III secretion: *Salmonella* SipA injection into host cells. *Proc Natl Acad Sci USA* **102:** 12548–12553.

Schraidt, O., and Marlovits, T.C. (2011) Three-dimensional model of *Salmonella's* needle complex at subnanometer resolution. *Science* **331:** 1192–1195.

Sory, M.P., and Cornelis, G.R. (1994) Translocation of a hybrid YopE-adenylate cyclase from *Yersinia enterocolitica* into HeLa cells. *Mol Microbiol* **14:** 583–594.

Sory, M.P., Boland, A., Lambermont, I., and Cornelis, G.R. (1995) Identification of the YopE and YopH domains required for secretion and internalization into the cytosol of macrophages, using the cyaA gene fusion approach. *Proc Natl Acad Sci U S A* **92:** 11998–12002.

Stainier, I., Iriarte, M., and Cornelis, G.R. (1997) YscM1 and YscM2, two *Yersinia enterocolitica* proteins causing down-regulation of yop transcription. *Mol Microbiol* **26:** 833–843.

Veenendaal, A.K., Hodgkinson, J.L., Schwarzer, L., Stabat, D., Zenk, S.F., and Blocker, A.J. (2007) The type III secretion system needle tip complex mediates host cell sensing and translocon insertion. *Mol Microbiol* **63:** 1719–1730.

Viprey, V., Del Greco, A., Golinowski, W., Broughton, W.J., and Perret, X. (1998) Symbiotic implications of type III protein secretion machinery in Rhizobium. *Mol Microbiol* **28:** 1381–1389.

Yother, J., and Goguen, J.D. (1985) Isolation and characterization of Ca2+-blind mutants of *Yersinia pestis*. *J Bacteriol* **164:** 704–711.

## Supporting information

Additional supporting information may be found in the online version of this article at the publisher's web-site.